

Solution combustion synthesis of zinc and calcium aluminate spinel phase materials: optical and structural properties

K Mahi¹, G Benabdellah^{1*} , K El Assad Zemallach Ouari² and M Trari³

¹ Laboratory of Physical Engineering, Department of Physics, Faculty of Matter Sciences, University of Tiaret, Tiaret, Algeria

² Département de Physique, Faculté des Sciences Exactes, Université Mostapha Stambouli, BP 305, Mamounia, Mascara, Algeria

³ Laboratory of Storage and Valorization of Renewable Energies, USTHB, BP 32, 16111 Algiers, Algeria

Received: 07 October 2023 / Accepted: 28 March 2024

Abstract: In this experimental study, zinc aluminate and calcium aluminate spinel nano-powders were synthesized using the solution combustion method. Subsequently, we explored the impact of metal cation substitution (Zn^{+2} and Ca^{+2}) on the optical and structural properties of these samples through ultraviolet–visible (UV–Vis) spectroscopy, Fourier transform infrared spectroscopy (FT-IR), and X-ray diffraction analysis (XRD). Crystalline forms of $ZnAl_2O_4$ and $CaAl_2O_4$ were obtained after calcination at 900 °C for 4 h under atmospheric air conditions. The UV–visible spectroscopy results revealed optical bandgap values of 3.771 and 3.507 eV for $ZnAl_2O_4$ and $CaAl_2O_4$ respectively. The FT-IR spectra demonstrated the presence of intense fundamental absorption peaks in the wavenumbers range 400–745 cm^{-1} , confirming the formation of metal aluminate spinel structure. The X-ray diffraction analysis confirmed the spinel structure of the prepared samples. Furthermore, the XRD results revealed that the variation of the M element in the structure led to change in the lattice type and the crystallite size, which is ranged from 26.003 to 42.001 nm. These findings indicate that these compounds are promising candidates for a range of optoelectronic applications.

Keywords: Nanomaterials; Spinel; Synthesis; XRD; FT-IR; UV–visible spectroscopy

1. Introduction

Spinel-type materials have garnered considerable attention from researchers in recent years owing to their unique properties and extensive array of applications [1–6]. This heightened interest stems from their remarkable characteristics, which make them versatile candidates for various technological and scientific endeavors. Spinel-type is known by its general chemical formula, which is written as AB_2O_4 , where A and B are divalent and trivalent metal cations respectively, and O is the oxygen ions [7–11], the cations A and B are occupying tetrahedral and octahedral sites within the crystal lattice. Generally, the crystal structure of spinel-type is closely resembles that known structure of the mineral spinel $MgAl_2O_4$ [8]. The diverse range of properties exhibited by these materials is influenced by the method of preparation and the specific

transition metal cations employed, particularly their coordination within the crystal structure. Among spinel-type materials, the M-based aluminate spinel MA_2O_4 , where M is divalent metal cations (such as Mg^{2+} , Cr^{2+} , Mn^{2+} , Co^{2+} , Ni^{2+} , Cu^{2+} , or Zn^{2+}), are present many advantages such as large surface area, high mechanical and thermal resistance, thermal stability, hydrophobic behavior, high melting point, wide band-gap energy and optical transparency [1, 2, 4, 12–15]. The latter property facilitates the generation of free radicals for advanced oxidation processes (AOPs), which are responsible for photocatalytic reactions.

The experimental investigation of spinel-type nanoceramics involves the synthesis, characterization and application of these materials in various contexts. Researchers employ a multitude of techniques and methodologies to explore their unique properties and potential applications in various fields, as manufacturing of electronic devices, catalysis materials and energy storage [16, 17]. The nano spinel-type can be synthesized from a mixture of oxides via different methods such as solid-state reactions [18, 19], oil-in-water [20], freeze-drying [21], combustion synthesis [22],

*Corresponding author, E-mail: gghlamallah.benabdellah@univ-tiaret.dz

sol–gel technique [23, 24], spray drying [25] and sonochemical process [26]. The solution combustion method is a versatile and relatively simple technique extensively employed for synthesizing a wide array of nano-sized ceramic materials [22]. Generally, this method involves the exothermic reaction between the reactants as a sol–gel or aqueous solution which leading to the formation of the desired products. Its efficiency is particularly notable in the production of ceramics, intermetallic compounds, and mixed oxides and sulfides alloys [27]. One of the key advantages of this method is the precise control of the chemical composition of the synthesized samples with a good crystallinity, a perfect homogeneity and a high purity. Moreover the properties of the synthesized samples such as the average crystallite size, lattice parameter, interplanar spacing, structure type, functional groups of chemical bonds and energy band gap can be influenced by a several factors such as the method and conditions of synthesis, choice of organic fuel and solvent, initial precursor quantities, nature of the substituting element, and dopant concentration [28, 29].

The aim of this research is to experimentally investigate the influence of metal cations on the structural parameters and optical properties of aluminate spinel compounds MA_2O_4 , with zinc (Zn) and calcium (Ca) atoms selected as the M elements. The samples of MA_2O_4 were synthesized using the solution combustion method at room temperature. The solution combustion method is a useful technique to synthesize spinel-type aluminate nanopowders using simple equipment. To characterize the final products of zinc aluminate and calcium aluminate nanopowders, we have used the available techniques in our laboratory which are: ultraviolet–visible spectroscopy (UV–Vis), Fourier-transform infrared spectroscopy (FT-IR), and X-ray diffraction (XRD).

2. Experimental background

2.1. Synthesis of aluminate nanopowders

In this work, the aluminate $ZnAl_2O_4$ and $CaAl_2O_4$ nanopowders were prepared using the solution combustion method [22]. The process involved the utilization of zinc nitrate hexahydrate, calcium nitrate tetrahydrate, aluminum nitrate nonahydrate (obtained from Sigma Aldrich with a purity of 99.99%), and urea. The urea $CO(NH_2)_2$ is used as fuel due to its important role in the synthesis process, specifically, urea, featuring amine (NH_2) and carbonyl ($C=O$) groups, possesses the capability to potentially form hydrogen bonds with the surface oxygen atoms of spinel-type oxides. Moreover, urea serves as a catalyzing agent in the synthesis of precursors crucial for spinel-type

oxide formation. The chemical formulas of these substances and the used stoichiometric proportions in this study are summarized in Table 1.

The synthesis procedure involved preparing homogeneous solutions of the substances in distilled water, followed by stirring for 6 h at room temperature (300 K). Finally, the $ZnAl_2O_4$ and $CaAl_2O_4$ powders were obtained through heat treatment at a calcining temperature of 900 °C for 4 h in an air atmosphere. At 900 °C, the thermal energy is sufficient to initiate the decomposition of the precursor compounds and promote the rearrangement of atoms into the desired crystalline structures of $ZnAl_2O_4$ and $CaAl_2O_4$. Additionally, this temperature ensures the removal of any residual organic matter from the precursor materials, resulting in the formation of pure and well-defined spinel powders.

The complete procedure for solution combustion synthesis of zinc aluminate and calcium aluminate nanopowders is illustrated in Fig. 1, detailing each step involved in the synthesis process, including precursor mixing, thermal agitation, drying, calcination, and product formation.

2.2. Measurements

Optical properties and band gap energy of the prepared powders were investigated from Tauc's plots using the absorbance spectra of ultraviolet–visible diffuse reflectance spectroscopy (SHIMADZU UV-1650-PC). Chemical characterization of the powder samples was carried by analysis of Fourier transform infrared spectra recorded by an Alpha Bruker FT-IR spectrometer in the wavenumber range between 350 and 4000 cm^{-1} . The composition phase and crystal structure of zinc aluminate and calcium aluminate spinel's nanopowders were examined from the X-ray diffraction (XRD) patterns obtained by MiniFlex 600 powder diffractometer with $Cu_{K\alpha}$ radiation, $\lambda = 1.5406 \text{ \AA}$, in the range from 2° to 90° with a step of 0.01° at room temperature.

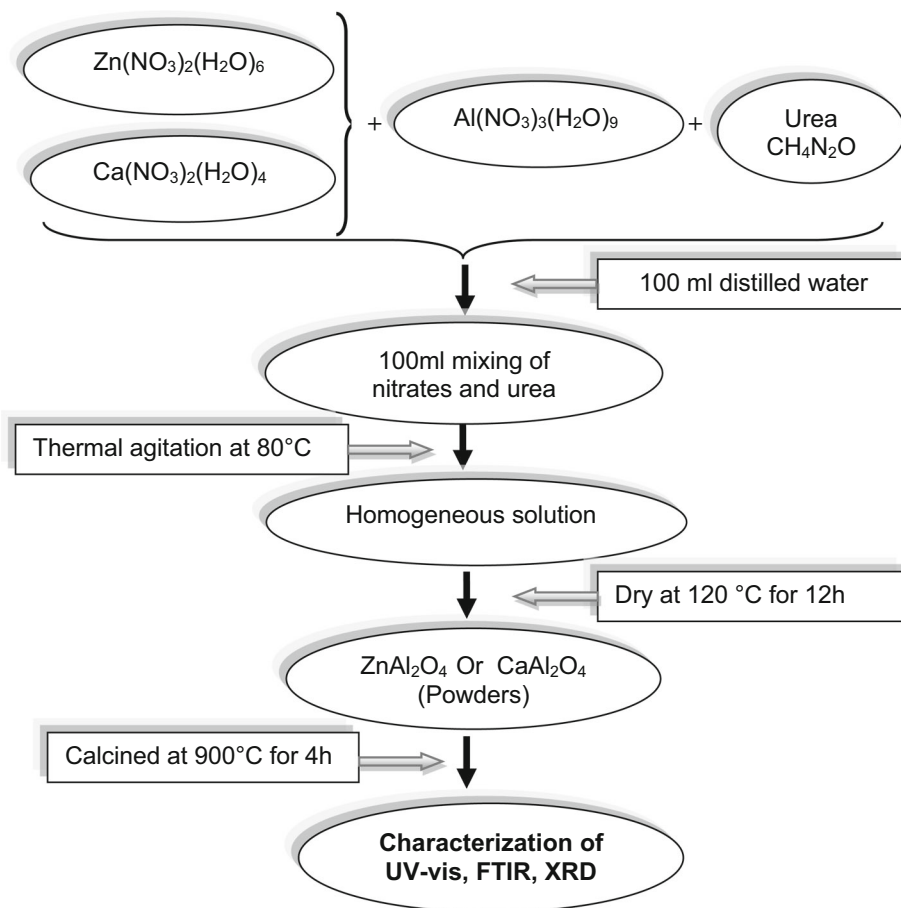
3. Results and discussion

3.1. Optical properties

To study the optical properties of $ZnAl_2O_4$ and $CaAl_2O_4$ samples, which are prepared by the solution combustion method, we have performed UV–Vis measurements in the range from 200 to 900 nm, the obtained results are depicted in Figs. 2 and 3. We can clearly see from these figures that the absorbance spectrum of $ZnAl_2O_4$ sample presents a strong narrow absorption peak at $\lambda_{max} = 310 \text{ nm}$ (in the UV region), this absorption is due to the electronic excitation between filled 2p-O states and empty 4s state of

Table 1 Stoichiometric proportions and chemical formulas of the raw materials used in the preparation of 100 mL of solutions

Name of compound	Chemical formula	Physical form	Color	Quantities used (g)
Aluminum nitrate	$\text{Al}(\text{NO}_3)_3(\text{H}_2\text{O})_9$	Powder	White	5.000
Zinc nitrate	$\text{Zn}(\text{NO}_3)_2(\text{H}_2\text{O})_6$	Powder	White to colorless	2.170
Calcium nitrate	$\text{Ca}(\text{NO}_3)_2(\text{H}_2\text{O})_4$	Granular	White or grey	1.575
Urea	$\text{CH}_4\text{N}_2\text{O}$	Granular	Colorless	4.560

Fig. 1 Schematic diagram for solution combustion synthesis process of ZnAl_2O_4 and CaAl_2O_4 

transition metal Zn [30], while the absorbance spectrum of CaAl_2O_4 sample shows a large band absorption with a principal peak located at $\lambda_{\text{max}} = 250$ nm in the UV region, this large band absorption bands was explained by the fundamental electron transition between filled 2p-O states and empty 3 s-Al states [13]. The compounds not absorbing in the visible range are those with full or empty d orbitals of elements in the absorption and are transparent to UV light. The optical absorbance spectrum of our ZnAl_2O_4 solution appears narrower compared to the spectrum obtained for ZnAl_2O_4 powders prepared via the hydrothermal method [30]. However, our peak absorption aligns well with the high absorbance observed in the 250 to

400 nm region at ambient temperature [30]. The wide peak observed for CaAl_2O_4 compared to ZnAl_2O_4 in the UV-Vis measurements could be attributed to several factors. For example, the presence of defects, impurities, or structural disorders in the crystal lattice of CaAl_2O_4 can affect the electronic band structure and lead to broader absorption peaks in the UV-Vis spectrum. These defects may introduce additional energy levels within the band gap, resulting in enhanced absorption over a broader range of wavelengths.

It is well known that the optical band gap can be calculated from UV-Vis spectra by using the empirical Tauc's

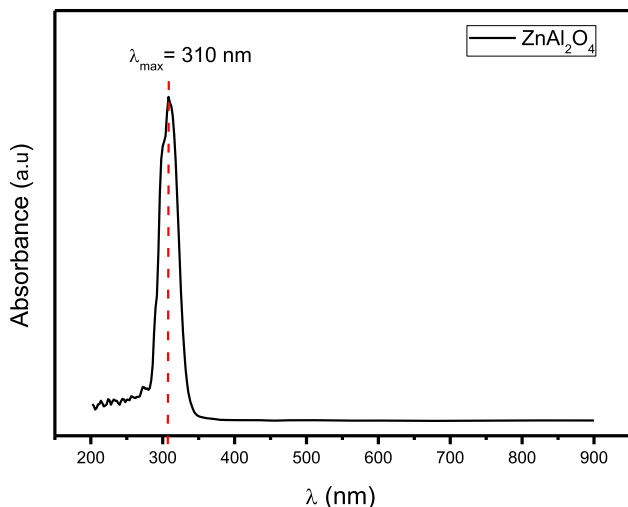


Fig. 2 Absorbance spectrum (in arbitrary unit) of the ZnAl_2O_4 nanoparticles calcined at 900°C for 4 h

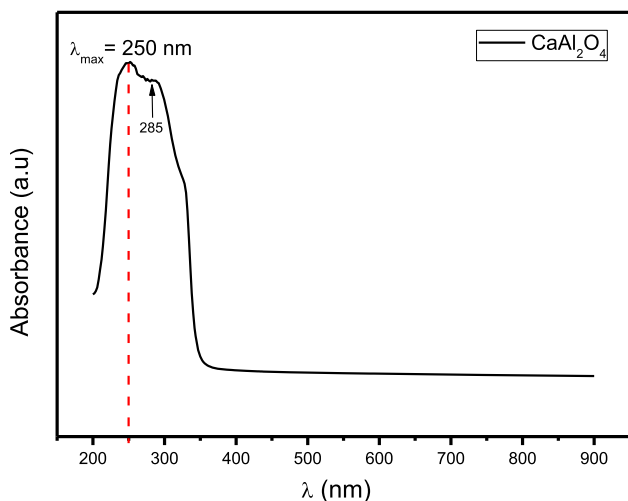


Fig. 3 Absorbance spectrum (in arbitrary unit) of the CaAl_2O_4 nanoparticles calcined at 900°C for 4 h

model [31], which is expressed by the following formula [32, 33]:

$$(\alpha h\nu)^n = A(h\nu - E_g) \quad (1)$$

where $(h\nu)$ is the photon energy, α is the absorption coefficient, A is a constant, E_g is the optical band gap of the sample and the exponent n associated the type of electronic transition ($n = 1/2, 2, 1/3,$ and 3 for direct and indirect optical transition).

The value of E_g is evaluated from the intercept of the tangent with the x-axis ($h\nu$) of the Tauc's plots [34], which is displayed as the variation of $(\alpha h\nu)^n$ versus of the photon energy $h\nu$ with $n = 2$ for direct band gap as shown in Figs. 4 and 5.

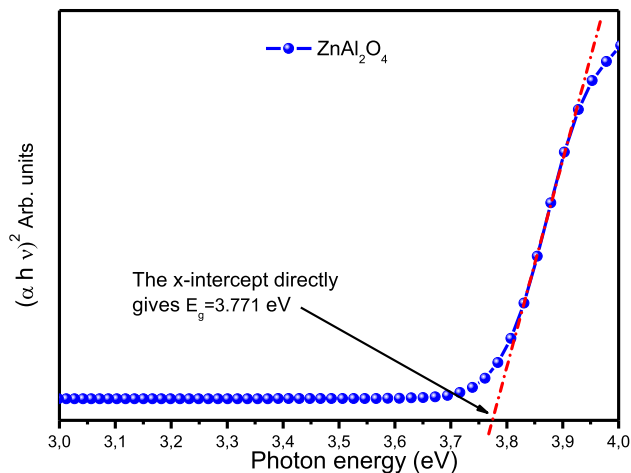


Fig. 4 Plot of the quantity $(\alpha h\nu)^2$ versus photon energy ($h\nu$) obtained from the absorbance spectrum of Fig. 2 for zinc aluminate

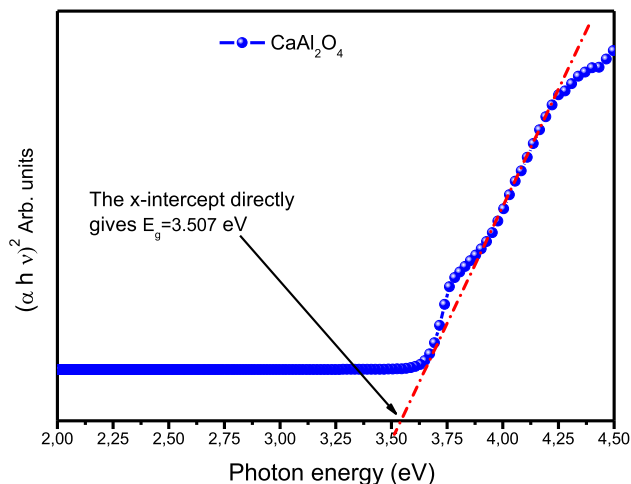


Fig. 5 Plot of the quantity $(\alpha h\nu)^2$ versus photon energy ($h\nu$) obtained from the absorbance spectrum of Fig. 3 for calcium aluminate

Theoretically, we employ the value $n = 2$ in our case to indicate a direct transition. However, the d–d transition, attributed to the crystal field splitting of Zn^{2+} and Ca^{2+} in the tetrahedral site of the spinel, is not observed, despite the presence of the transition metal with an incomplete 3d orbital, which typically results in colored oxides. This transition is forbidden by the Laporte law [35]. The results indicate that our prepared ZnAl_2O_4 metal spinel solution exhibits a direct band gap value of 3.771 eV, slightly lower than reported value of $E_g = 3.9$ eV for zinc aluminate powders prepared by the solution combustion method with glycine-urea mixed as fuel [36]. However, Theophil Anand et al. [37] found a larger band gap value of 5.05 eV using the microwave combustion technique to prepare their samples. Our prepared calcium aluminate solution also exhibits a direct band gap value of 3.507 eV, which is lower than the value of $E_g = 5.0$ eV reported by Kumar

et al. [13] for calcium aluminate nanopowders prepared by using a facile self-propagating solution combustion synthesis with oxalyldihydrazide as fuel, and the value of $E_g = 5.6$ eV reported by Mabelane et al. [38] for the same compound prepared via the citrate sol-gel method. Furthermore, it is evident that the band gap energy (E_g) values of zinc aluminate and calcium aluminate nanopowders are influenced by the chosen preparation technique.

3.2. FT-IR studies

Fourier transform infrared spectroscopy (FT-IR) is a versatile analytical technique that provides valuable insights into the bonding mechanisms in organic or inorganic material. Its applications span various scientific disciplines and industries. In this work, we have used FT-IR to identify the formation of spinel structure and the nature of the functional groups of chemical bonds in nanoparticles of studied samples. Figures 6 and 7, show the infrared spectrums of zinc aluminate and calcium aluminate nanoparticles in the range of 350 to 4000 cm^{-1} . In view of these FT-IR spectra of ZnAl_2O_4 and CaAl_2O_4 calcined samples, we can observe several weak absorption peaks around positions 450.31, 492.48, 618.99, 1441.33, 1546.76, 2295.30, and 3170.36 cm^{-1} . Three prominent vibrational peaks located at around positions 450.31 cm^{-1} , 492.48 cm^{-1} , and 618.99 cm^{-1} suggest the formation of zinc aluminate and calcium aluminate spinel structures. However, the broad absorption bands in wavenumbers ranging from 3100 cm^{-1} to 3650 cm^{-1} correspond to symmetric and asymmetric vibration modes of water molecules ($-\text{OH}$) [39]. The other absorption peaks located at the wavenumbers 1441.33 cm^{-1} and 1546.76 cm^{-1} are attributed to carbon-oxygen bonds, such as C-O and C=O [40].

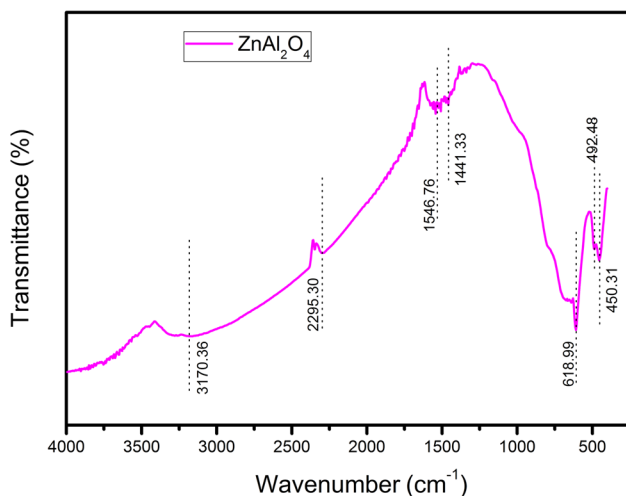


Fig. 6 FT-IR spectrum of ZnAl_2O_4 sample prepared via solution combustion synthesis process and calcined at 900 °C for 4 h

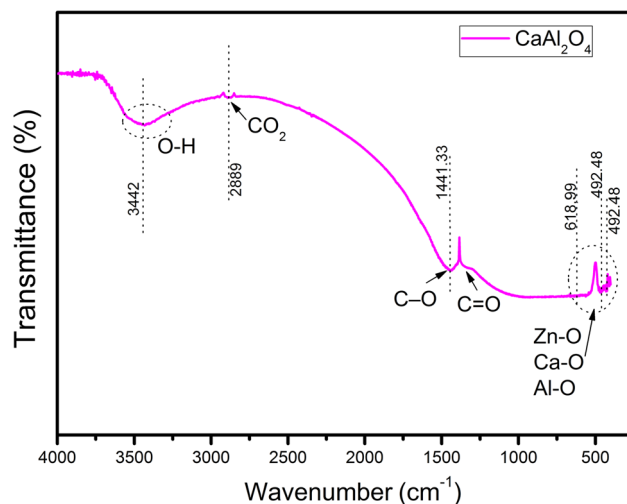


Fig. 7 FT-IR spectrum of CaAl_2O_4 sample prepared via solution combustion synthesis process and calcined at 900 °C for 4 h

Meanwhile, the weak peak observed at 2295.30 cm^{-1} is related to the presence of CO_2 on the sample's surface [40–42].

3.3. Phase and structural analysis

The phase composition and crystal structure of zinc aluminate and calcium aluminate nanopowders were identified through the XRD measurements at ambient temperature. The nanopowders samples were prepared after 4 h of calcination at temperature of 900 °C. Figures 8 and 9 show the obtained XRD patterns, we should note here that all observed XRD peaks of aluminate samples are match excellently with ICSD (Inorganic Crystal Structure Database) PDF Card No. 01-074-1138 and 20-02-888, indicating the high-purity and crystalline structure of the prepared

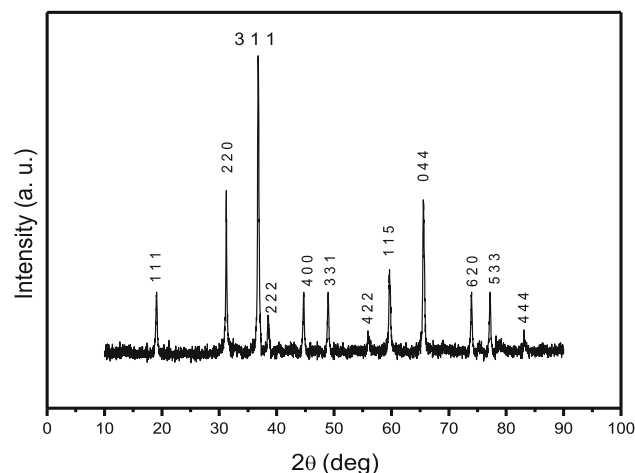


Fig. 8 XRD pattern of zinc aluminate the nanocrystals calcined at 900 °C for 4 h

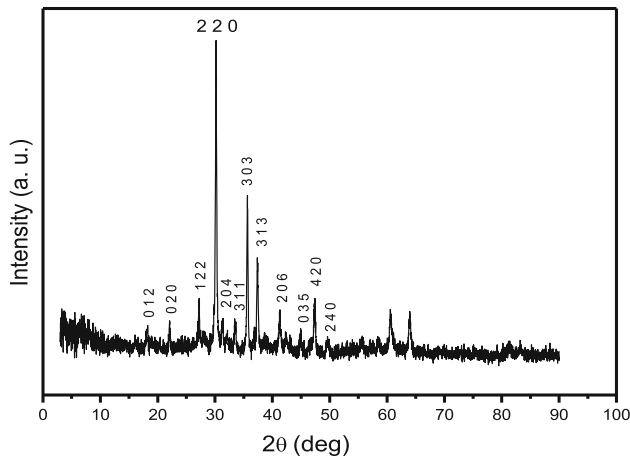


Fig. 9 XRD pattern of calcium aluminate the nanocrystals calcined at 900 °C for 4 h

powders. For ZnAl_2O_4 nanoparticles the peaks at 2θ values are located at 18.964°, 31.211°, 36.775°, 38.474°, 44.722°, 48.985°, 55.543°, 59.235°, 65.099°, 73.960°, 77.171°, and 82.439°. According ICSD database, these peaks correspond respectively to (111), (220), (311), (222), (400), (331), (422), (115), (044), (620), (533) and (444) diffraction planes. Whereas the CaAl_2O_4 sample present a different peaks and diffraction planes compared to ZnAl_2O_4 sample. For this latter, the dominant peaks are located at 2θ values of 15,991°, 21,955°, 26,984°, 30,140°, 31,295°, 33,341°, 35,699°, 37,442°, 41,283°, 44,902°, 47,421°, and 49,662° correspond to (012), (020), (122), (220), (204), (311), (303), (313), (206), (035), (420), and (240) diffraction planes, respectively. The major phase in these structures of ZnAl_2O_4 and CaAl_2O_4 nanoparticles exhibits a moderately crystalline nature. Zinc oxide (Zn–O), calcium oxide (Ca–O), and aluminum oxide (Al_2O_3) were not clearly observed in the XRD pattern analysis of calcined nanopowders. The obtained XRD patterns of zinc aluminate and calcium aluminate nanopowders confirm the formation of cubic and monoclinic spinel phase with space group Fd-3 m and P21/n, respectively.

From the XRD measurement data, we can also investigate other important parameters, such as lattice parameter, cell volume, interplanar spacing and the average crystallite size of our prepared samples. The average crystallite size D of the prepared powders can be calculated by the following empirical Debye–Scherrer formula [43, 44]:

$$D = \frac{L\lambda}{B \cos(\theta_{hkl})} \quad (2)$$

where L is the crystallite shape factor (equal to 0.9), λ is the X-ray wavelength ($\lambda = 0.154059$ nm), θ_{hkl} is the maximum of the Bragg diffraction peak (in radians) and B is the full width at half maximum intensity (FWHM).

For cubic system, the lattice parameter a can be calculated by the following formulas [29, 45]:

$$a = d_{hkl} \sqrt{h^2 + k^2 + l} \quad (3)$$

where d_{hkl} is interplanar spacing, it can be calculated by using the following Bragg formula:

$$d_{hkl} = \frac{\lambda}{2 \sin(\theta_{hkl})} \quad (4)$$

($h k l$) are the Miller indices of the plane, λ is the wavelength of X ray source and θ is the diffraction angle corresponding to the most intense reflection plane. The conventional cell volume (V) can be calculated from the lattice parameter of cubic system by the simple relation $V = a^3$.

For monoclinic system, the interplanar spacing are related to the lattice parameters a , b and c and the angle β by the following formulas:

$$\frac{1}{d_{hkl}^2} = \frac{1}{\sin^2(\beta)} \left(\left(\frac{h}{a} \right)^2 + \left(\frac{k \sin(\beta)}{b} \right)^2 + \left(\frac{l}{c} \right)^2 - \frac{2hl \cos(\beta)}{ac} \right) \quad (5)$$

And the conventional cell volume is written as: $V = a \cdot b \cdot c \cdot \sin(\beta)$.

The computed parameters from the XDR pattern analysis are summarized in Table 2. The average crystallite sizes of CaAl_2O_4 and ZnAl_2O_4 are 26.0 and 42.0 nm respectively. The results of the lattice parameter and average crystallite sizes of ZnAl_2O_4 powders are in good agreement with those reported by T. Tangcharoen et al. ($a = 8.092$ Å and $D = 42$ nm calcined at 1000°C) [46]. It has been found that the average crystallite size and lattice parameter increase when the calcination temperature is enhanced, promoting the crystal core formation reaction within a short time[12, 46].

Table 2 Structural parameters extracted from XRD analysis for ZnAl_2O_4 and CaAl_2O_4 samples

Parameters	ZnAl_2O_4	CaAl_2O_4
Crystal structure type	Cubic	monoclinic
Space group	Fd-3 m	P21/n
Lattice parameters	$a = 8.099$ Å	$a = 8.700$ Å $b = 8.092$ Å $c = 15.191$ Å $\alpha = \gamma = 90^\circ$ $\beta = 90.17^\circ$
Crystallite size (nm)	42.001	26.003
Cell volume (Å ³)	531.24	1069.448

4. Conclusion

The ZnAl₂O₄ and CaAl₂O₄ aluminate spinel nanopowders were successfully synthesized using the solution combustion method. Subsequently, the resulting nanocrystals underwent calcination at 900 °C for 4 h and were subsequently subjected to analysis using UV–Vis, FT-IR, and XRD techniques. Crystallographic analysis of XRD patterns shows the formation of spinel phase for both compounds. In addition, the lattice type, the cell volume and the average crystallite size changes of the samples follow M (Zn and Ca) metal cation changes. The appearance of peaks in the frequency range 450 cm⁻¹ and 650 cm⁻¹ in the IR spectra of both samples confirms the formation of spinel structures. The results from UV–visible diffuse reflectance spectroscopy determine distinct optical band gap of 3.771 eV and 3.507 eV for the ZnAl₂O₄ and CaAl₂O₄ samples, respectively. It's clearly that such values depend on the nature of the substituting element. All characterization results suggested that the prepared ZnAl₂O₄ and CaAl₂O₄ powders can be potential candidates for diverse applications such as hydrogen production, nuclear waste, photocatalysts, refractory materials, energy storage, photovoltaics and photodetectors.

References

- [1] Y Song and Y L Zheng *Sci. Forum* **898** 1935 (2017)
- [2] Q Wang, Q Chang and Y Wang *Lett.* **173** 64 (2016)
- [3] M Amiri, M Salavati-Niasari and A Pardakhty *Sci. Eng. C* **76** 1085 (2017)
- [4] M A Yousuf, M M Baig, N F Al-Khalli and M A Khan *Int.* **45** 10936 (2019)
- [5] W Lv, B Liu, Q Qiu, F Wang and Z Luo *J. Alloys Compd.* **479** 480 (2009)
- [6] L-W Zhang *Funct. Mater.* **17** 3781 (2007)
- [7] M Salavati-Niasari and F Davar *Mater. Lett.* **63** 441 (2009)
- [8] K E Sickafus *J. Am. Ceram. Soc.* **82** 3279 (2004)
- [9] R Tiwari and M De H S Tewari and S K Ghoshal *Results Phys.* **16** 102916 (2020)
- [10] T T Ahmed *J. Mater. Process. Technol.* **153–154** 797 (2004)
- [11] A Sutka and G Mezinskis *Mater. Sci.* **6** 128 (2012)
- [12] R Ianoş *Eng. J.* **240** 260 (2014)
- [13] K V Kumar *J. Nano Sci. Eng.* **05** 68 (2015)
- [14] M R Quirino, M J C Oliveira, D Keyson and G L Lucena *Res. Bull.* **74** 124 (2016)
- [15] A H Wako *J. Rare Earths* **32** 806 (2014)
- [16] A Manikandan *Sci. Eng. Med.* **7** 33 (2015)
- [17] G Padmapriya, A Manikandan and V Krishnasamy *J. Supercond. Nov. Magn.* **29** 2141 (2016)
- [18] L T T Vien, N Tu, M T Tran, N Van Du, D H Nguyen, D X Viet and N V Quang *Mater.* **100** 109670 (2020)
- [19] C Gómez-Solís, S L Peralta-Arriaga and L M Torres-Martínez *Juárez-Ramírez and L A Díaz-Torres Fuel* **188** 197 (2017)
- [20] A E Giannakas and A K Ladavos *Surf. Sci.* **253** 6969 (2007)
- [21] C-T Wang *J. Am. Ceram. Soc.* **75** 2240 (1992)
- [22] M Sundararajan, M Sukumar, C S Dash, A Sutha, S Suresh, M Ubaidullah and A M Al-Enizi *B Condens. Matter* **644** 414232 (2022)
- [23] S Maitra *Appl. Phys.* **20** 628 (2020)
- [24] A M Mansour *Nano-Objects* **25** 100646 (2021)
- [25] A Douy and M Capron *J. Eur. Ceram. Soc.* **23** 2075 (2003)
- [26] M Jamdar, R Monsef, S H Ganduh and E A Dawi *Environ. Saf.* **269** 115801 (2024)
- [27] E Carlos, R Martins, E Fortunato and R Branquinho *Chem. – Eur. J.* **26** 9099 (2020)
- [28] F Li and J Ran *M Jaroniec and S Z Qiao Nanoscale* **7** 17590 (2015)
- [29] F Deganello and A K Tyagi *Prog. Cryst. Growth Charact. Mater.* **64** 23 (2018)
- [30] I Miron and C Enache *Scr.* **T149** 014064 (2012)
- [31] M Panahi-Kalamuei *J. Alloys Compd.* **617** 627 (2014)
- [32] A Kadari, K Mahi and L O Faria *J. Phys.* **55** 127 (2017)
- [33] M Muralidharan and S Selvakumar *B Condens. Matter* **615** 413039 (2021)
- [34] M Ashraf and S M J Akhtar *Phys. J. Appl. Phys.* **48** 10501 (2009)
- [35] O Laporte and W F Meggers *J. Opt. Soc. Am.* **11** 459 (1925)
- [36] S A Mirbagheri *S M Masoudpanah and S Alamolhoda Optik* **204** 164170 (2020)
- [37] G T Anand, L J Kennedy and J J Vijaya *Int.* **41** 603 (2015)
- [38] T S Mabelane, L F Koao, S V Motloung and T E Motaung *J. Mol. Struct.* **1260** 132751 (2022)
- [39] M Jafari and S A Hassanzadeh-Tabrizi *Powder Technol.* **266** 236 (2014)
- [40] C Ragupathi and J J Vijaya *P Surendhar and L J Kennedy Polyhedron* **72** 1 (2014)
- [41] H Teymourinia and M Salavati-Niasari *J. Mol. Liq.* **242** 447 (2017)
- [42] M Salavati-Niasari *M Dadkhah and F Davar Polyhedron* **28** 3005 (2009)
- [43] M Sivagami and I V Asharani *Inorg. Chem. Commun.* **145** 110054 (2022)
- [44] A A Othman and M A Osman *B Condens. Matter* **614** 413041 (2021)
- [45] S Peddarasi and D Sarkar *Mater. Chem. Phys.* **262** 124275 (2021)
- [46] T Tangcharoen *J. Adv. Ceram.* **8** 352 (2019)

Publisher's Note Springer Nature remains neutral with regard to jurisdictional claims in published maps and institutional affiliations.

Springer Nature or its licensor (e.g. a society or other partner) holds exclusive rights to this article under a publishing agreement with the author(s) or other rightsholder(s); author self-archiving of the accepted manuscript version of this article is solely governed by the terms of such publishing agreement and applicable law.